Hysteretic Energy Dissipation Capacity of Dual-Steel Welded-Plate Preloaded Bolted T-stubs

Fangxin Hu[a,b,*], Tao Lin[a], Zhan Wang[a,b]

[a]*School of Civil Engineering and Transportation, South China University of Technology, Guangzhou, 510640, China*
[b]*State Key Laboratory of Subtropical Building Science, South China University of Technology, Guangzhou, 510640, China*

Abstract

With the high- and ultrahigh-strength steels applied in the construction industry, the seismic safety of their structural components are very concerned due to the inferior material ductility of those steels. The current studies on bolted high-strength steel T-stubs mainly focus on their monotonic loading behavior. There is limited research work conducted to study their cyclic loading behavior. In this study, cyclic tests of bolted dual-steel T-stubs were conducted. Their T-elements were produced by Q690 high-strength steel flanges and Q355 normal-strength steel webs, and class 10.9 high-strength bolts with pretension were used to connect the groove-welded T-elements. Failure modes, force–deformation hysteretic and backbone curves, cumulative plastic deformation and energy dissipation capacities were tested and analyzed. The test results indicated that an optimal β ratio between the plastic resistances of Mode 1 (neglecting the influence of bolt action on a finite contact area) and Mode 3 in Eurocode 3 Part 1-8 could be 0.3 for those bolted T-stubs to maximize hysteretic energy dissipation. Accordingly, predictive formulas with good precision were proposed for the low-cycle fatigue failure criterion and hysteretic energy dissipation capacity of those bolted T-stubs, respectively.

Keywords: Bolted T-stub, Dual-steel, High-strength steel, Hysteretic energy, Cyclic, Welded plate

---

*Corresponding author
Email address: `hufx@scut.edu.cn` (Fangxin Hu)

1 Introduction

In recent years, there has been an emerging trend to use high-strength steel with a nominal yield strength not less than 460 MPa in the construction industry to gain additional specific strength, good economic benefits and environmental friendliness compared to conventional low-carbon mild and low-alloy steels [1–6]. In general, welded moment connections are widely used in seismic resistant steel structures [7, 8]. However, it was not easy to ensure the weld of high-strength steel with the same strength as the base metal due to the softening effect observed in the heat affected zone (HAZ) [9, 10]. Sometimes, field-bolted connections are strongly recommended, and even required, for rapid construction to reduce the construction cycle and simultaneously the associated costs. Therefore, some commonly used field-bolted connection types, such as bolted extended and flush end-plate connections, bolted T-stub connections and bolted angle connections, may be utilized to connect high-strength steel members and components [11–15]. Particularly, mild steel is always used in energy dissipative members (e.g. beams and/or braces), while high-strength steel is preferred in the other members that have to remain predominantly elastic, such as columns [16]. Such a case between mild steel beams and high-strength steel columns leads to dual-steel bolted joints. Furthermore, the structural behavior of those bolted joints can be characterized using the component method in Eurocode 3 Part 1-8 [17], and the equivalent T-stub subjected to tension and compression is one of the basic components. Note that earthquake hazard has been one of the most critical factors to threaten the safety of steel structures, and the cyclic behavior of bolted dual-steel or high-strength steel T-stubs are crucial to evaluate its joint and structural behavior.

In the last few decades, many researchers have performed experimental and numerical studies on the structural behavior of bolted dual-steel or high-strength steel T-stubs under monotonic loading [11, 18–32]. The previous results revealed the effects of steel grades, welding-induced softening in the HAZ, post-weld heat treatment, combined loading of tension and shear, and placement of stiffeners on the initial stiffness and plastic resistance of bolted T-stubs. Some contradictory conclusions were found, and so, through a recent study by the authors [31], it was generally concluded that the softening effect in the HAZ may be related to the steel production technique as well as the welding process, and if this softening can be ignored or alleviated, the current formulae in Eurocode 3 Part 1-8 can be still applied to bolted high-strength steel T-stubs in terms of the initial stiffness, plastic resistance and joint modeling approach. However, limited studies were conducted to evaluate the cyclic behavior. Dubina et al. [19, 20] and Muntean et al. [21] performed cyclic testing on dual-steel bolted T-stubs between grade S235 webs and grade S460 or S690 flanges. They found that compared with the steel grades, the types of failure mode (flange bending, bolt rupture, or combined mode) had much larger influence on the ductility, and the ductility was largely decreased by cyclic loading when the failure mode was dominated by flange bending. But in the loading history they used the compression force was limited to avoid buckling, which may underestimate the cyclic damage under earthquakes. Kleiner and Kuhlmann [22] conducted experimental studies on two series of bolted dual-steel T-stubs, one group being unstiffened T-stubs and the other being stiffened T-stubs, where web plates were all made of mild steel while S460 or S690 steel end plates were used. The specimens were designed aiming at a Mode 2 failure (bolt failure with flange yielding) in Eurocode 3 Part 1-8, but to exhibit ductile (close to Mode 1, or say, flange yielding) and brittle (close to Mode 3, or say, bolt failure) mechanisms, respectively. However, it was found that the cyclic loading history did not affect much on the ultimate resistance and ductility of those T-stubs when compared with the results under monotonic loading. This was due to the relatively thick end plates (even in the ductile mode), which made the ultimate performance basically dominated by the identical bolts used in this study. The knowledge on the real cyclic bending deformation capacity of high-strength steel end plates was still limited. Chen et al. [32] reported experimental and numerical studies on cyclic performance of Q460 and Q690 high-strength steel bolted T-stubs. They found by the experimental study that using the same bolts, the increase of the flange thickness aided energy dissipation, and by the numerical study they further confirmed the probable existence of an flange thickness to maximize energy dissipation. But their numerical study did not take into account the ultimate failure in the flange or bolts, neither did they present any criteria to evaluate the capacity of energy dissipation.

As described previously, there is still no available method to evaluate the energy dissipation capacity of high-strength steel bolted T-stubs. The authors thus report an experimental program consisting of ten bolted dual-steel T-stub specimens fabricated by Q355 steel webs and Q690 high-strength steel flanges in China that were subjected to cyclic loading of both constant and variable amplitudes. The main variable considered in this study was the Q690 flange thickness, while class 10.9 high-strength bolts of a nominal diameter of 20 mm (M20) were always used. The test results will be presented in terms of hysteretic and backbone force-deformation curves as well as low-cycle fatigue curves. Accordingly, a curve fit to predict the hysteretic energy dissipation capacity will be proposed.

2 Test program

2.1 T-stub specimens

A series of ten cyclic tests on bolted T-stub specimens made of welded grade Q355 (f_y = 355 MPa) normal-strength and grade Q690 high-strength steels was conducted. In each T-stub specimen, two identical T-elements was connected by a pair of preloaded class 10.9 high-strength bolts of a nominal diameter of 20 mm (denoted as M20), as shown in Figure 1. So, only one bolt row was considered. The steel grade and thickness of the flange plates in the T-stubs varied in this study, as shown in Table 1, while the web plates were all made of 14 mm-thick grade Q355 steel plates. In this way, those specimens were typical of dual-steel T-stubs that are representative components in bolted beam-to-column connections, such as in extended end-plate connections using Q690 end plates between Q355 beams and Q690 columns [15]. The dimensions are shown in Figure 1 and Table 1. Note that the web plate was welded to the flange plate using a continuous complete penetration K-type groove weld. This is the case for the connection between the end plate and beam flanges in a bolted end-plate joint as required by Chinese Specification [33]. Each specimen is given a name for ease of reference, which starts with T indicating T-stubs and a number to represent the flange thickness (in mm), followed by V or C indicating variable-amplitude or constant-amplitude loading, respectively. The number after C is the amplitude magnitude (in mm). Details of the loading amplitudes will be introduced in the following Section 2.3. For example, Specimen T10-V represents a specimen that used 10 mm-thick flange plates and was subjected to variable-amplitude cyclic loading, while Specimen T10-C5 represents a specimen that used 10 mm-thick flange plates and was subjected to cyclic loading with a constant amplitude of 5 mm in deformation.

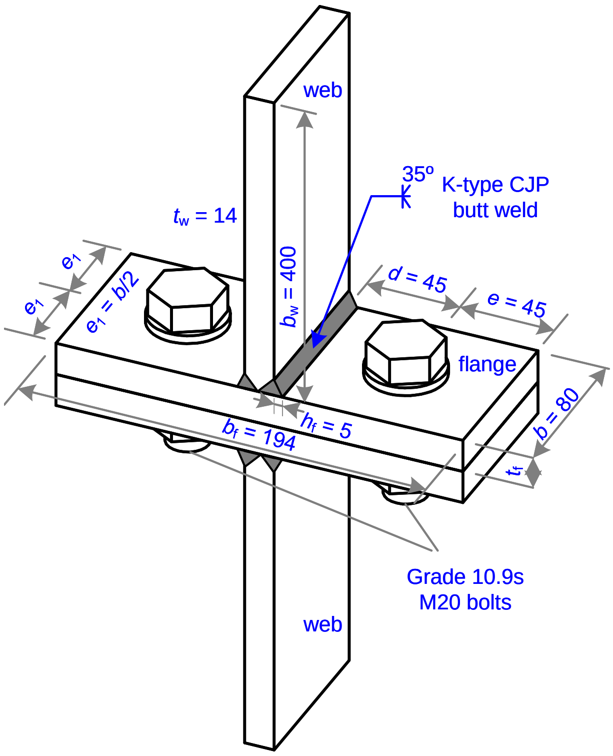

Figure 1. T-stub geometry (unit: mm)

T-stubs may exhibit different failure modes, depending on the flexural resistance of the flange and the tensile resistance of the bolt. According to Eurocode 3 Part 1-8, three collapse mechanisms

Table 1. Test specimens

Specimen label	b (mm)	t_f (mm)	b_f (mm)	t_w (mm)	b_w (mm)	d (mm)	e (mm)	β	Amplitude (mm)
T8-V T8-C7 T8-C11 T8-C15	80	8	194	14	400	45	45	0.18	Variable 7 11 15
T10-V T10-C5 T10-C13	80	10	194	14	400	45	45	0.31	Variable 5 13
T12-V T12-C9 T12-C13	80	12	194	14	400	45	45	0.44	Variable 9 13

can be identified, and the corresponding plastic resistances are

$$F_{\mathrm{p1}} = \frac{(32n - 2d_{\mathrm{wsh}})\, M_{\mathrm{pf}}}{8mn - (m+n)\, d_{\mathrm{wsh}}} \tag{1a}$$

$$F_{\mathrm{p2}} = \frac{2M_{\mathrm{pf}} + 2nB}{m+n} \tag{1b}$$

$$F_{\mathrm{p3}} = 2B \tag{1c}$$

where the influence of the bolt action on a finite contact area is taken into account in Mode 1 collapse; $M_{\mathrm{pf}} = b_{\mathrm{eff}} t_{\mathrm{f}}^2 f_{\mathrm{y}}/4$ is the plastic flexural resistance of the T-stub flange, where b_{eff} is the effective width, which is the minimum value provided by both the circular and non-circular patterns for collapse Mode 1 and that corresponding only to the non-circular pattern for collapse Mode 2, f_{y} is the yield strength of the flange material; d_{wsh} is the diameter of the washer; m is the distance between the bolt axis and the conjunction (weld toe) of the flange and web where the formation of a plastic hinge is expected, and $m = d - 0.8h_{\mathrm{f}}$ where d is the distance from the bolt axis to the web face and h_{f} is the weld throat height equal to 5 mm, as shown in Figure 1; n is the effective edge distance, which is the minimum value between e (the distance between the bolt axis and the tip of the flanges, as shown in Figure 1) and $1.25m$; $B = 0.9 f_{\mathrm{ub}} A_{\mathrm{e}}$ is the axial plastic resistance of a single bolt in tension, where f_{ub} is the ultimate tensile strength of the bolt material (nominally 1000 MPa for class 10.9 bolts) and A_e is the effective tensile area of the bolt (245 mm^2 for M20 bolts). The collapse mode is determined by the relative strength between the flange and bolt, and can be characterized by

$$\beta = \frac{2M_{pf}}{Bm} \tag{2}$$

Thus, it was easily verified that all the three flange thicknesses in Table 1 were characterized by Mode 1 collapse, i.e., only yielding and plastic bending in the flanges. The β ratios for the specimens, calculated using the measured material properties in the following subsection, are also shown in Table 1. This was intentionally designed so that the plastic deformation and energy dissipation capacity of the high-strength steel T-stub flange under cyclic bending could be assessed. In case of the ultimate failure controlled by bolt rupture in Mode 2 or Mode 3 rather than flange fracture, the effect of cyclic loading should be insignificant, as already evidenced by the previous studies [19, 22].

2.2 Material properties

The steel materials used in this study are identical to a previous study by the authors [31]. The mechanical properties of the Q690 steel used in the T-stub flanges are shown in Table 2, where E is the elastic modulus, f_y is the yield strength, f_u is the ultimate strength, ϵ_{st} is the strain at the end of the yield plateau, ϵ_u is the ultimate strain, and δ is the elongation after fracture. The corresponding stress–strain curves are shown in Figure 2. Note that the 8 mm– and 10 mm–thick Q690 steel plates did not exhibit any distinct yield plateau in their stress–strain curves. In these cases, the yield strength is the proof stress corresponding to a residual plastic strain of 0.2%.

Tension test on the class 10.9 high-strength bolt was also conducted to obtain its elastic modulus E, ultimate strength f_u and ultimate strain ϵ_u, as shown in Table 2. The measured diameter of the washers (d_w) used with those class 10.9 M20 high-strength bolts was about 38.4 mm. Manual gas shielding arc welding using a consumable electrode of grade E50, which fits to

Table 2. Material properties

Steel Gr.	Plate thickness (mm)	E (GPa)	f_y (MPa)	f_u (MPa)	ϵ_{st}	ϵ_u	δ (%)
Q690	8	208.3	723	822	—	0.100	20
	10	189.4	794	902	—	0.106	21
	12	205.8	775	816	0.018	0.060	16
10.9s	M20	206.0	—	1135	—	0.110	—

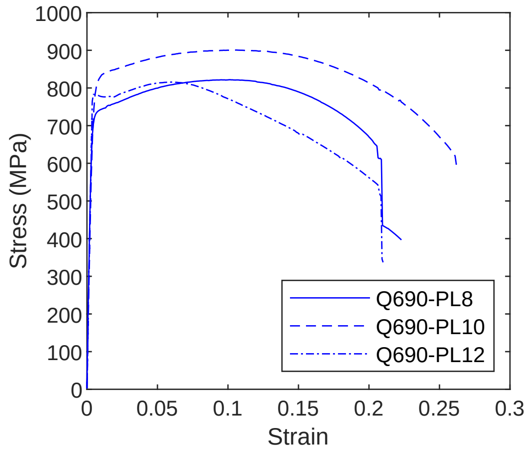

Figure 2. Q690 steel stress-strain curves

Q355 normal-strength steel, was adopted for the groove welds between the T-stub webs and flanges. Since the T-stub webs only transfer the axial load to the flanges, the material properties of the T-stub webs were not measured.

2.3 Test setup and procedures

Before the formal test, the class 10.9 high-strength bolts in the T-stub specimens were tightened by a torque wrench to achieve a design preload of 155 kN according to Chinese Specification [33]. The specimens were then placed into a servo-hydraulic universal test machine and aligned, so that the grips were centered with respect to the T-stub webs, as shown in Fig. 3. Cyclic loading tests were performed with displacement control until failure, while the opening gap between the flanges was monitored by a displacement transducer at the centerline of the webs. In constant-amplitude tests the measured opening gap was loaded to the target amplitude in tension, and was reversed to zero in compression. In variable-amplitude tests, at the first stage the measured opening gap was loaded to 5 mm in tension and then reversed to zero; the tension amplitude was incremented by 2 mm in every subsequent stage but the compression amplitude was always kept as zero. Note that three cycles were implemented at each stage. These cyclic loading histories well replicate the situation for T-stubs when the prototype bolted beam-to-column joint is subjected to symmetric cyclic reversals of constant or variable amplitudes.

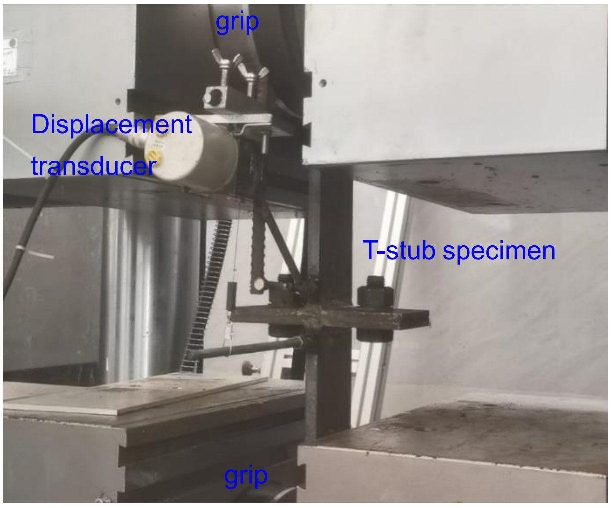

Figure 3. Test setup

3 Test results

3.1 Failure modes

All the T-stub specimens were designed to undergo Model 1 failure. Thus, they all experienced cracking in the HAZ of the flange near the weld between the flange and web plates, and such cracking finally induced total fracture of the flange, as shown in Figure 4 for typical tests. The cracking process, along with loud noises, however, was difficult to trace accurately. Therefore, only final complete fracture of the flange is summarized here. For Specimen T8-V, the flange completely fractured when the opening gap reached 13 mm at the second cycle of 15 mm amplitude, and a major crack was observed in the other flange. For Specimens T8-C7, T8-C11,

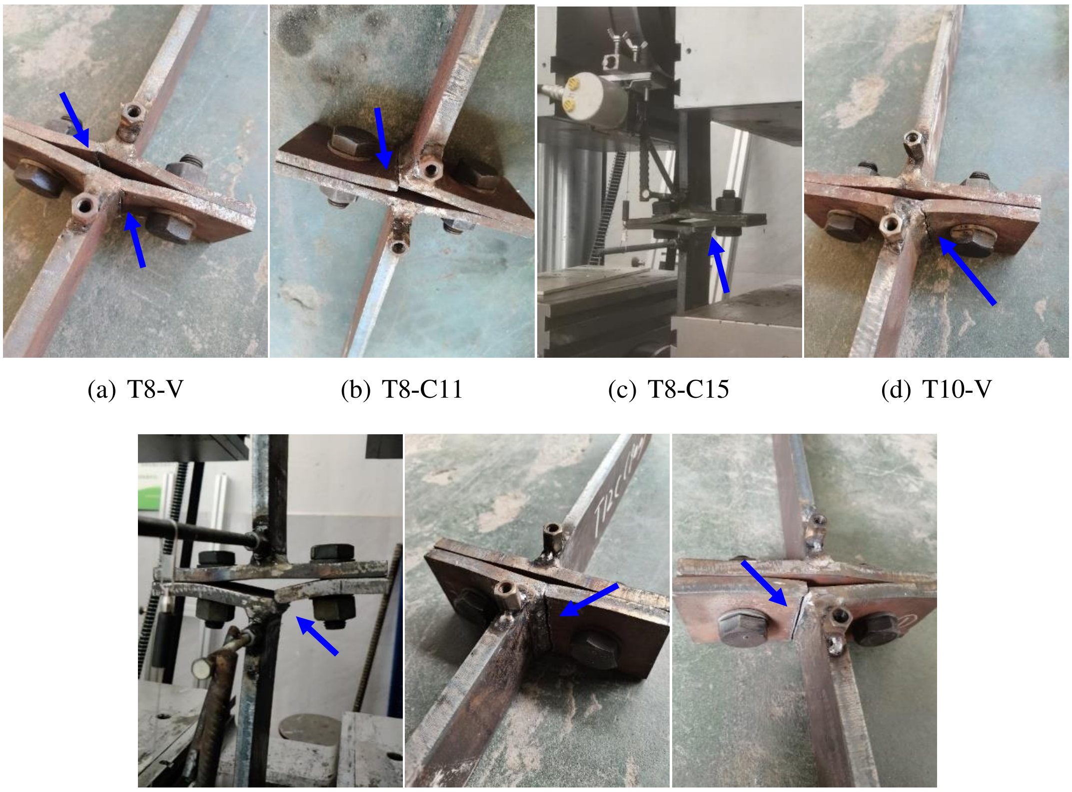

(a) T8-V (b) T8-C11 (c) T8-C15 (d) T10-V

(e) T12-V (f) T12-C9 (g) T12-C13

Figure 4. Typical failure modes

and T8-C15, complete fracture in the flange was noticed when the opening gap reached 6 mm, 6 mm, and 7 mm, at the 25th, 10th, and 7th cycle, respectively. Similarly, for Specimen T10-V, the flange completely fractured when the opening gap reached 9 mm at the second cycle of 13 mm amplitude. For Specimens T10-C5 and T10-C13, complete fracture in the flange was noticed when the opening gap reached the corresponding tension amplitude at the 61st and 8th cycle, respectively. Lastly, for Specimen T12-V, the flange completely fractured when the opening gap reached 11 mm at the second cycle of 13 mm amplitude, while for Specimens T12-C9 and T12-C13, complete fracture in the flange was noticed when the opening gap reached 6 mm and 13 mm at the 20th and 5th cycle, respectively.

3.2 Hysteretic and backbone curves

Axial force–deformation hysteretic curves of all the tested T-stub specimens are shown in Figure 5, where the deformation is the measured opening gap between the flanges at the web centerline. The moments of complete flange fracture are also marked in the figure, along with the number of cycle when the fracture occurred. It is clear that as the flange thickness increases from 8 mm to 12 mm, pinching effect in the hysteretic curves becomes more apparent. This is because the thicker the flange, the larger the bolt deformation (elongation and flexure), which introduces a significant slippage stage in the curves under unloading from tension and reloading into compression. Cyclic degradation of both stiffness and strength are also apparent in the curves, due to crack initiation and its associated propagation in the flanges. In addition, shown in Figure 6 are backbone curves from the hysteretic curves under variable-amplitude loading only, that were constructed by connecting the first loading branch with subsequent tension amplitudes. It is clear that the thicker the flange, the higher the ultimate (maximum) strength. And this maximum strength was reached at the deformation of 9 mm for the three specimens (T8-V, T10-V and T12-V).

3.3 Strength, ductility and energy dissipation

According to the method recommended by ECCS [34], the yield point was detected in the backbone curve based on the intersection of an initial straight line whose slope is the initial stiffness, and a subsequent tangent line to the curve whose slope is one-tenth of the initial stiffness. Due to the highly nonlinear initial branch of the backbone curve, the initial stiffness (K) was obtained by a linear fit to the first unloading branch after the achievement of 5 mm deformation in each variable-amplitude hysteretic curve. The axial force and deformation at the yield point were then defined as the yield strength (F_y) and deformation (δ_y), respectively, as shown in Table 3. The ultimate strength (F_u) was easily obtained as the maximum force in the backbone curves. The ultimate deformation (δ_u) was counted only if a least one complete cycle of

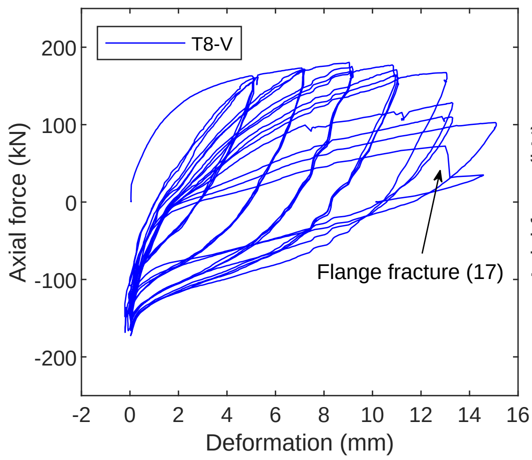

(a) T8-V

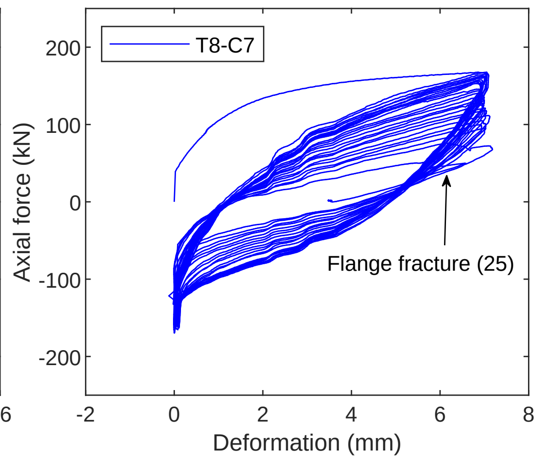

(b) T8-C7

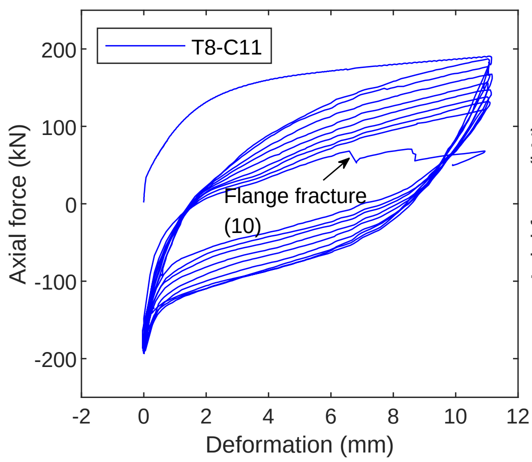

(c) T8-C11

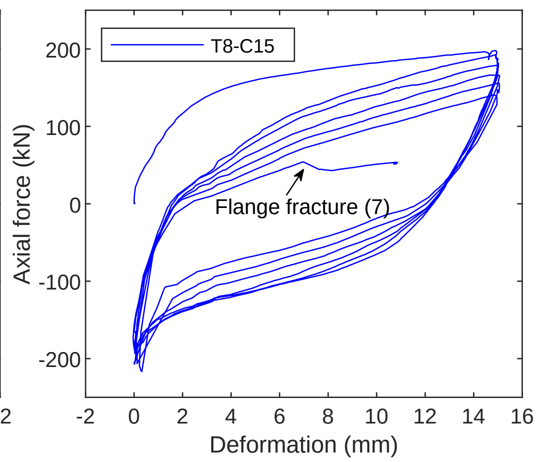

(d) T8-C15

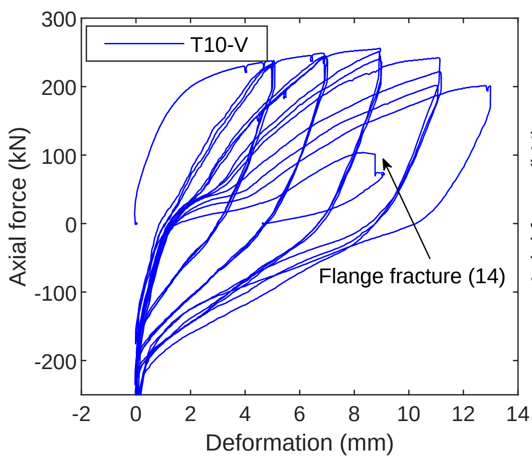

(e) T10-V

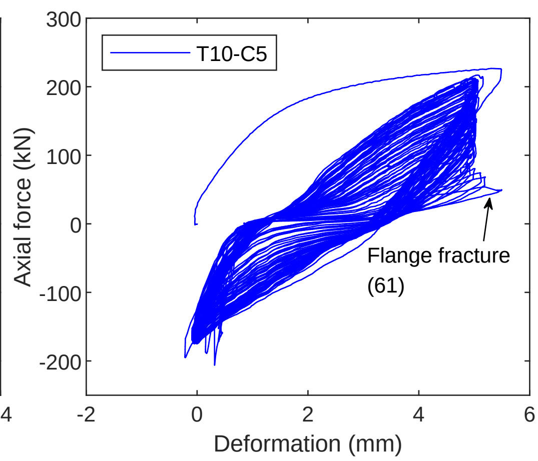

(f) T10-C5

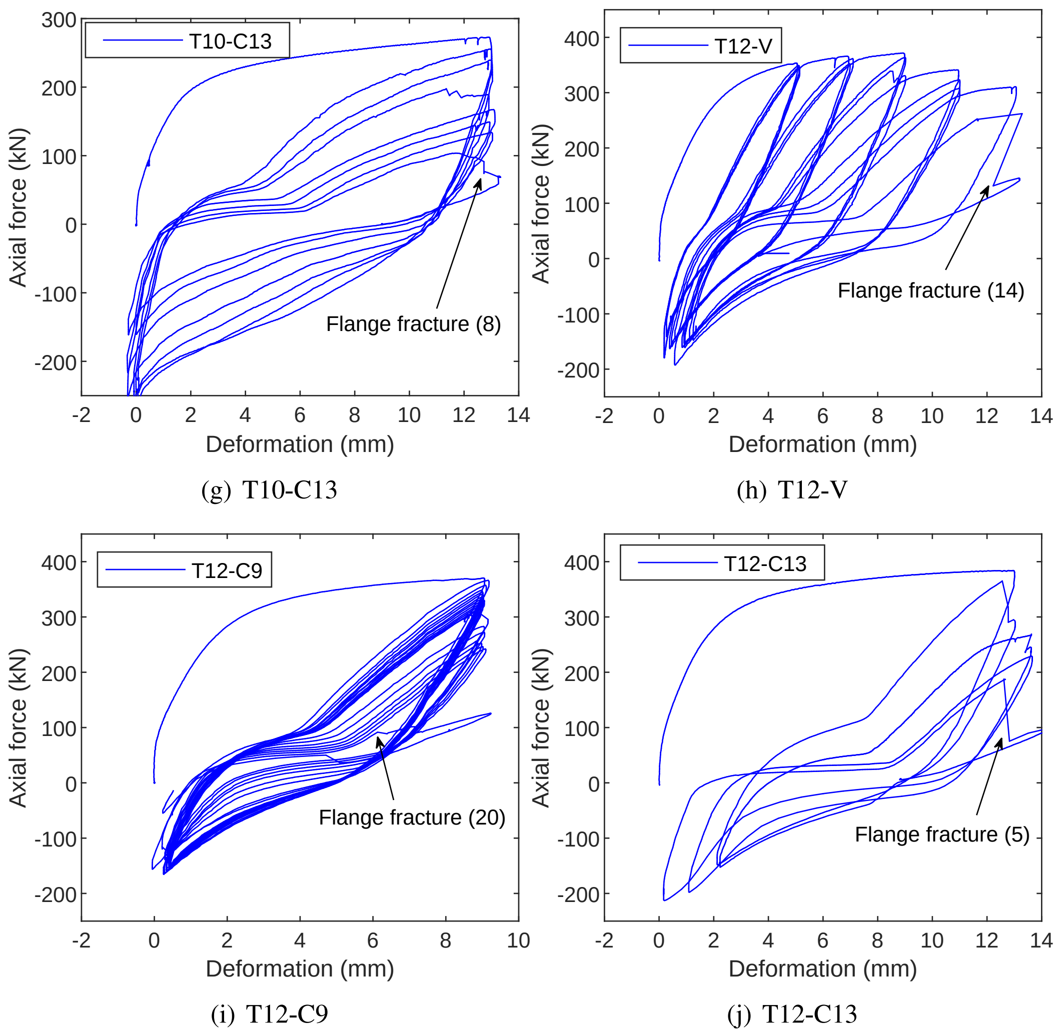

(g) T10-C13
(h) T12-V
(i) T12-C9
(j) T12-C13

Figure 5. Axial force–deformation hysteretic curves

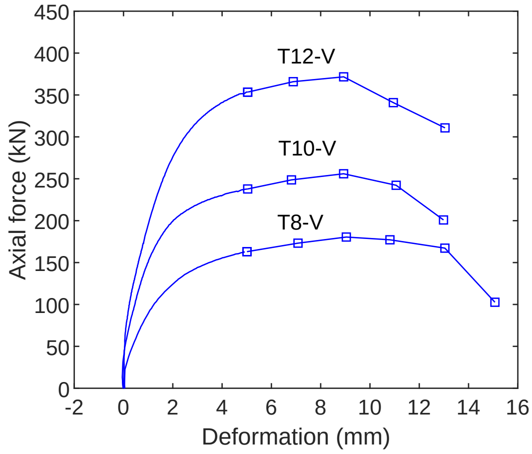

Figure 6. Axial force–deformation backbone curves

the target deformation amplitude was completed before total flange fracture or bolt rupture occurred. For example, Specimen T8-V failed by complete flange fracture at the second cycle of 15 mm amplitude in tension, then its ultimate deformation was taken as 15 mm. The calculated plastic resistance (F_p) based on Eurocode 3 Part 1-8, which was obtained by Eq. (1a) as Mode 1 dominated collapse, is shown in Table 3. As shown clearly, the ratios between the test yield and calculated plastic strength (F_y/F_p) range from 0.77 to 0.92, demonstrating conservatism in the theoretical method. This evidences that the formulae in Eurocode 3 Part 1-8 can be still applied to Q690 high-strength steel, which is in accordance with the findings in the previous studies [31, 32]. Besides, the overstrength (F_u/F_y) revealed by the tests ranges from 1.19 to 1.26, and it generally increases with the decrease of the flange thickness.

Table 3. Stiffness, strength and ductility

Specimen label	K (kN/mm)	F_y (kN)	F_u (kN)	F_u/F_y	F_p (kN)	F_p/F_y	δ_y (mm)	δ_u (mm)	μ
T8-V	69.8	142.8	180.5	1.26	110.1	0.77	2.05	15	7.3
T10-V	116.3	205.9	256.0	1.24	188.9	0.92	1.77	13	7.3
T12-V	149.2	312.9	371.6	1.19	265.6	0.85	2.10	13	6.2

The ductility factor, μ, defined as δ_u/δ_y, was also calculated and is shown in Table 3. Its values range from 6 to 7, indicating good ductility. In order to further examine the deformation capacity under cyclic loading, the maximum plastic deformation amplitude, δ_{p}, cumulative plastic deformation, $\Sigma\Delta\delta_{\mathrm{p}}$, and energy dissipation, ΣA, of all the specimens were determined based on the method in ATC-24 [35], as shown in Figure 7. Those values were counted until the last successful excursion (or half-cycle) before complete flange fracture or bolt rupture occurred, as summarized in Table 4. The normalized cumulative plastic deformation by the plastic deformation amplitude, $\Sigma\Delta\delta_{\mathrm{p}}/\delta_{\mathrm{p}}$, is also included in this table. It should be mentioned that for the easiness of comparison, the plastic deformation amplitudes for three variable-amplitude tests were directly taken as those in the constant-amplitude tests of the same ultimate total deformation. It is clear that those cumulative quantities are highly variable in the constant-amplitude tests, and generally, the cumulative plastic deformation ($\Sigma\Delta\delta_{\mathrm{p}}$ or $\Sigma\Delta\delta_{\mathrm{p}}/\delta_{\mathrm{p}}$) and energy dissipation (ΣA) both decrease with the increase of loading amplitude. Besides, the plastic deformation quantities (μ, δ_{p}, $\Sigma\Delta\delta_{\mathrm{p}}$, and $\Sigma\Delta\delta_{\mathrm{p}}/\delta_{\mathrm{p}}$) revealed by the variable-amplitude tests all show a decreasing trend with the increase in flange thickness. This is reasonable since the specimens failed all by collapse Mode 1, and more plastic rotation, associated with the axial plastic deformation of the whole T-stub, could be tolerated by thinner flanges. But the total energy dissipated under the same variable-amplitude cyclic history actually shows a maximum (16.8 kJ) if the flange thickness is an intermediate value (10 mm), slightly higher than that (16.2 kJ) if the flange thickness is 8 mm but obviously more than that (13.4 kJ) if the flange thickness is 12 mm. This suggests an optimal balance in proportioning the flange and bolt to maximize energy dissipation capacity. In this study, such an optimal balance may be achieved in Specimen T10-V by setting β as 0.3 (see Table 1). Such a result is in accordance with the conclusion in a previous study by the authors on the maximum ductility under monotonic loading [31]. But further study on more specimens is still needed for evidence.

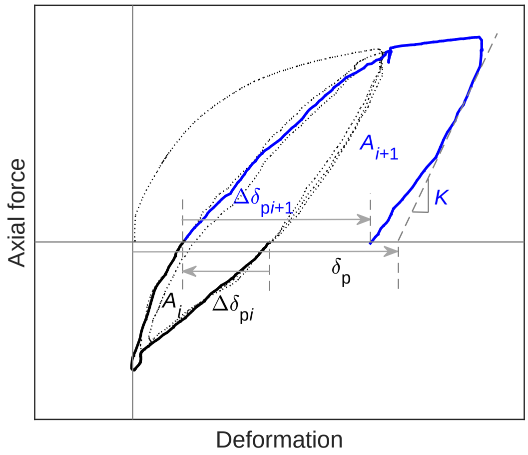

Figure 7. Definition of plastic deformation amplitude, cumulative plastic deformation and energy dissipation

4 Discussions

4.1 Low-cycle fatigue curves

Low-cycle fatigue of steel structural components, including the bolted T-stubs examined in this study, can be captured by a Coffin-Manson type relationship as [36, 37]

$$\delta_{\mathrm{p}} = aN_{\mathrm{f}}^{b} \tag{3}$$

where δ_{p} is the plastic deformation amplitude (see Table 4), N_{f} is the number of complete cycles before failure, a and b are coefficients related to structural details. Three constant-amplitude tests on the specimens with a flange thickness of 8 mm (T8-C7, T8-C11 and T8-C15) were conducted, and so a fit could be carried out directly on this flange thickness specimens, which led to values of 40.0 and −0.69 for a and b, respectively. Due to the limited number of constant-amplitude tests for the other two flange thickness specimens conducted in this study, all the specimens with three flange thicknesses were incorporated to fit the coefficients a and b, and the result is shown in Figure 8. The overall fitted values of a and b are 26.8 and −0.52, respectively. Such overall fitted result should not be reasonable enough since the flange thickness does have an impact on the

Table 4. Cumulative plastic deformation and energy dissipation

Specimen label	δ_p (mm)	$\Sigma\Delta\delta_p$ (mm)	$\Sigma\Delta\delta_p/\delta_p$	ΣA (kJ)
T8-V	12.32	169.9	13.8	16.2
T8-C7	4.63	163.9	35.4	13.7
T8-C11	8.30	119.1	14.4	11.4
T8-C15	12.32	126.7	10.3	13.6
T10-V	10.97	127.9	11.7	16.8
T10-C5	3.07	243.1	79.2	20.3
T10-C13	10.97	126.1	11.5	14.6
T12-V	10.50	74.9	7.1	13.4
T12-C9	6.53	107.6	16.5	16.5
T12-C13	10.50	54.1	5.2	8.3

plastic deformation capacity, and theoretically, the fit of Eq. (3) should be done for each group of specimens of individual flange thickness. But the overall fitted values of a and b in such a limited number of all the constant-amplitude tests still provide a clear picture on the fatigue performance of bolted T-stubs with high-strength steel flanges, if compared to that of normal-strength steel counterparts.

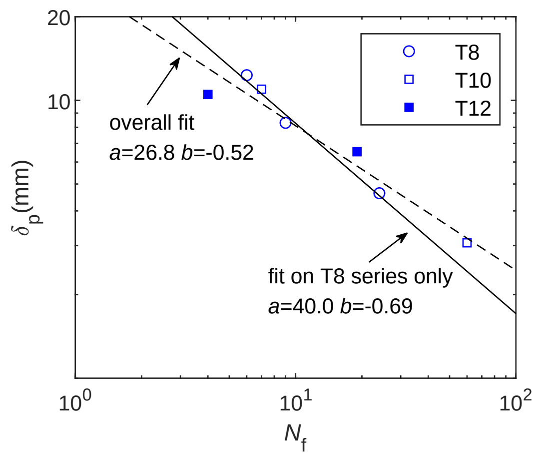

Figure 8. Low-cycle fatigue curves

Faella et al. [37, 38] have reported comprehensive cyclic test results on normal-strength steel (grade Fe430) T-stubs, using class 10.9 high-strength bolts with a pretension force equal to 0.80

times the bolt yield resistance. They found that the fitted coefficient a ranged from 86.1 to 136.3, and b ranged from −0.54 to −0.71, depending on the geometrical properties (HEA160 or HEA200 hot-rolled profiles) and also on the criterion used to define failure (50% degradation of, the maximum strength attained during each semicycle, the stiffness of the unloading branch of each semicycle, or the energy dissipated during each semicycle). Note that in this study the complete fracture of the flange or bolt was used to define the moment of failure. Therefore, the criterion used by Faella et al. [37] is absolutely conservative compared to the one used by the authors here. But it is interesting to notice that the fitted coefficient b here (−0.52 for overall fit, or −0.69 for T8 series only) are still very close to that range (−0.54 to −0.71) obtained for bolted normal-strength steel hot-rolled T-stubs. It seems that the steel grade does not affect much on the coefficient b, neither does the structural detail including the geometrical properties and type of profile. On the contrary, the coefficient a obtained here (26.8 for overall fit, or 40 for T8 series only) is substantially lower than the above corresponding range (86.1 to 136.3). It does make sense, as the coefficient a can be interpreted as the plastic deformation that can be achieved before failure under monotonic loading and is absolutely lower for high-strength steel as a result of its poorer material ductility than normal-strength steel. The welded-plate detail used in this study, if compared with the hot-rolled profile used in that previous study, contributed further to this large difference.

4.2 Hysteretic energy dissipation capacity

Table 4 shows that the total cumulative energy dissipation varies significantly among different cyclic loading amplitudes. Such a fact has already been recognized previously. In order to predict the hysteretic energy dissipation capacity, Faella et al. [37], Piluso and Rizzano [39] derived a method in their study on bolted normal-strength steel T-stubs. In their method, the hysteretic energy dissipation and plastic deformation amplitude are normalized before subsequent calibration. If the failure is controlled by flange fracture as in Model 1, the plastic deformation amplitude, δ_{p}, under a constant-amplitude cyclic loading, could be normalized by the ultimate plastic deformation that can be achieved under monotonic loading, $\delta_{\mathrm{p,th}}$. Faella et al. [38] and Piluso et al. [40, 41] proposed by theoretical derivation that

$$\delta_{\mathrm{p,th}} = \frac{m^2}{t_{\mathrm{f}}} C \tag{4}$$

where m and t_{f} have been illustrated in Section 2.1, C is a coefficient determined based on the stress–strain curve of the flange material. Then the normalized plastic deformation amplitude is

$$\bar{\delta} = \frac{\delta_{\mathrm{p}}}{\delta_{\mathrm{p,th}}} = \frac{\delta_{\mathrm{p}} t_{\mathrm{f}}}{2Cm^2} \tag{5}$$

Meanwhile, the cumulative hysteretic energy dissipation, E_{cc}, under the constant-amplitude cyclic loading, could be normalized by the energy dissipation achieved under monotonic loading until failure, E_0. That means, the normalized cumulative energy dissipation is

$$\bar{E} = \frac{E_{\mathrm{cc}}}{E_0} \tag{6}$$

In this way, an exponential relationship between $\bar{E}$ and $\bar{\delta}$ can be empirically determined as

$$\bar{E} = \psi_1 \bar{\delta}^{-\psi_2} \tag{7}$$

Substituting Eqs. (5) and (6) into Eq. (7) results in

$$\frac{E_{\mathrm{cc}}}{E_0} = \psi_1 \left(\frac{t_{\mathrm{f}} \delta_{\mathrm{p}}}{2Cm^2} \right)^{-\psi_2} = \bar{\psi}_1 \left(\frac{t_{\mathrm{f}} \delta_{\mathrm{p}}}{2m^2} \right)^{-\psi_2} \tag{8}$$

where $\bar{\psi}_1$ (or ψ_1) and ψ_2 are positive empirical coefficients that should be fitted by test results. Based on the test results of constant-amplitude loading in this study, the fit of Eq. (8) is shown in Figure 9. The fitted values of $\bar{\psi}_1$ and ψ_2 are 0.036 and 1.403, respectively. The coefficient of correlation is 0.89, indicating a good agreement. The fitted Eq. (8) can be used in predicting the cumulative hysteretic energy dissipation capacity of the dual-steel T-stubs.

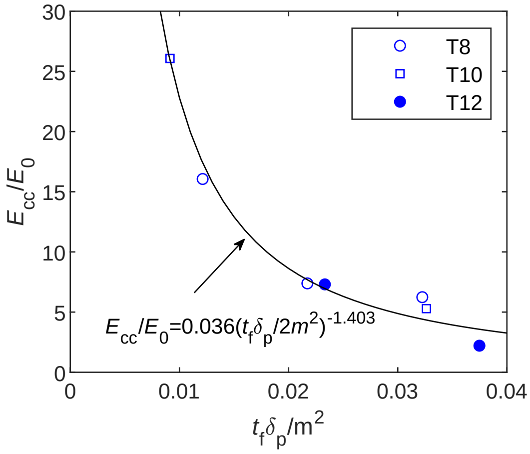

Figure 9. Normalized cumulative hysteretic energy dissipation–plastic deformation amplitude relationship

The above results can be further compared to those obtained for normal-strength steel (grade Fe430) T-stubs by Piluso and Rizzano [39]. In their study, for hot-rolled T-stubs, $\psi_1 = 2.081$ (or $\bar{\psi}_1 = 0.626 \sim 0.806$ based on $C = 0.371 \sim 0.457$) and $\psi_2 = 1.212$; for welded-plate T-stubs, $\psi_1 = 0.485$ (or $\bar{\psi}_1 = 0.157 \sim 0.167$ based on $C = 0.364 \sim 0.384$) and $\psi_2 = 1.117$. It is clear that, the coefficient ψ_2 fitted in this study (1.403) is slightly larger than the above results for normal-strength steel T-stubs, indicating a slightly increased rate of deterioration in cumulative energy dissipation capacity with the plastic deformation amplitude. In addition, the coefficient $\bar{\psi}_1$ fitted in this study (0.036) is significantly lower than those for normal-strength steel T-stubs (even lower than a range of $0.157 \sim 0.167$ for comparison on the basis of welded-plate T-stubs). This provides the evidence of lower energy dissipation capacity of dual-steel (or high-strength steel) T-stubs compared to normal-strength steel counterparts.

5 Conclusions

Cyclic testing of dual-steel welded-plate (Q355 web-Q690 flange) bolted T-stubs was conducted to evaluate their strength, ductility and energy dissipation. The T-stub specimens with three flange thicknesses were designed to undergo Mode 1 collapse (i.e., only flange yielding). A special emphasis was placed on the calibration of low-cycle fatigue curves and cumulative hysteretic energy dissipation capacity. Conclusions are as follows.

1) The plastic resistance formulae in Eurocode 3 Part 1-8 can be applied to the dual-steel (or high-strength steel) T-stubs, and is conservative to the yield resistance calibrated from the tests. The overstrength factor of the ultimate resistance is about 1.2.
2) The ductility of the dual-steel T-stubs ranges from 6 to 7. Both the ductility and the cumulative plastic deformation capacity increase with a decrease in the flange thickness.
3) The cumulative energy dissipation capacity is the maximum in case of an intermediate flange thickness, which corresponds to the β ratio (see Eq. (2)) of around 0.3.
4) Low-cycle fatigue failure of the dual-steel T-stubs could be roughly predicted by $\Delta\delta_{\mathrm{p}} = 26.8N_{\mathrm{f}}^{-0.52}$ (see Eq. (3)). More accurate equations on independent flange thickness deserve to be calibrated by further study.
5) Cumulative hysteretic energy dissipation capacity of the dual-steel T-stubs could be predicted by $E_{\mathrm{cc}}/E_0 = 0.036\left(t_{\mathrm{f}}\delta_{\mathrm{p}}/2m^2\right)^{-1.403}$ (see Eq. (8)).

Acknowledgments

The authors would like to acknowledge the financial supports for this work by the National Natural Science Foundation of China (Grant Nos. 51638009, 51978279 and 52108145).

References

[1] J. Raoul, H.-P. Günther, Use and application of high-performance steels for steel structures, International Association for Bridge and Structural Engineering (IABSE), Zürich, Switzerland, 2005.

[2] R. Bjorhovde, Development and use of high performance steel, Journal of Constructional Steel Research 60 (2004) 393–400.

[3] G. Shi, F. Hu, Y. Shi, Recent research advances of high strength steel structures and codification of design specification in China, International Journal of Steel Structures 14 (2014) 873–887.

[4] H. Ban, G. Shi, A review of research on high-strength steel structures, Proceedings of the Institution of Civil Engineers - Structures and Buildings 171 (2018) 625–641.

[5] G. Shi, X. Chen, Research advances in HSS structures at Tsinghua University and codification of the design specification, Steel Construction 11 (2018) 286–293.

[6] F. Hu, G. Shi, Constitutive model for full-range cyclic behavior of high strength steels without yield plateau, Construction and Building Materials 162 (2018) 596–607.

[7] F. Hu, G. Shi, Y. Shi, Experimental study on seismic behavior of high strength steel frames: Global response, Engineering Structures 131 (2017) 163–179.

[8] F. Hu, G. Shi, Experimental study on seismic behavior of high strength steel frames: Local response, Engineering Structures 229 (2021) 111620.

[9] F. Javidan, A. Heidarpour, X.-L. Zhao, C. R. Hutchinson, J. Minkkinen, Effect of weld on the mechanical properties of high strength and ultra-high strength steel tubes in fabricated hybrid sections, Engineering Structures 118 (2016) 16–27.

[10] R. M. Stroetmann, T. Kästner, B. Rust, Design and execution of welded connections on high-strength steels, Advances in Structural Engineering 0 (2023) 1–10.

[11] A. M. Girão Coelho, Characterization of the ductility of bolted end plate beam-to-column steel connections, Ph.D. thesis, University of Coimbra, Coimbra, Portugal, 2004.

[12] A. M. Girão Coelho, F. S. K. Bijlaard, Moment-resisting joints in high-strength steel: areas for improvement in design standards, Steel Construction 11 (2018) 294–305.

[13] A. M. Girão Coelho, F. S. K. Bijlaard, High strength steel in buildings and civil engineering structures: design of connections, Advances in Structural Engineering 13 (2010) 413–429.

[14] A. M. Girão Coelho, F. S. K. Bijlaard, Experimental behaviour of high strength steel end-plate connections, Journal of Constructional Steel Research 63 (2007) 1228–1240.

[15] T. Lin, Z. Wang, F. Hu, P. Wang, Finite-element analysis of high-strength steel extended end-plate connections under cyclic loading, Materials 15 (2022) 2912.

[16] D. Dubina, A. Stratan, C. Vulcu, A. Ciutina, High strength steel in seismic resistant building frames, Steel Construction 7 (2014) 173–177.

[17] European Committee for Standardization (CEN), Eurocode 3: Design of steel structures - Part 1-8: Design of joints. EN 1993-1-8:2005, British Standards Institution (BSI), London, UK, 2005.

[18] A. M. Girão Coelho, F. S. K. Bijlaard, N. Gresnigt, L. Simões da Silva, Experimental assessment of the behaviour of bolted T-stub connections made up of welded plates, Journal of Constructional Steel Research

60 (2004) 269–311.

[19] D. Dubina, A. Stratan, N. Muntean, D. Grecea, Dual-steel T-stub behaviour under monotonic and cyclic loading, in: R. Bjorhovde, F. S. K. Bijlaard, L. F. Geschwindner (Eds.), Proceedings of the Sixth International Workshop on Connections in Steel Structures VI, American Institute of Steel Construction, Chicago, Illinois, USA, 2008, pp. 185–196.

[20] D. Dubina, D. Grecea, A. Stratan, N. Muntean, Performance of dual-steel connections of high strength components under monotonic and cyclic loading, in: F. M. Mazzolani, J. M. Ricles, R. Sause (Eds.), Proceedings of the Sixth International Conference on Behaviour of Steel Structures in Seismic Areas (STESSA 2009), CRC Press/Balkema, Taylor & Francis Group, Philadelphia, Pennsylvania, USA, 2009, pp. 437–442.

[21] N. Muntean, D. Grecea, A. Dogariu, D. Dubina, Strength and ductility of bolted T-stub macro-components under monotonic and cyclic loading, in: E. Batista, P. Vellasco, L. de Lima (Eds.), Proceedings of the International Colloquium on Stability and Ductility of Steel Structures (SDSS'Rio 2010), Federal University of Rio de Janeiro and State University of Rio de Janeiro, Rio de Janeiro, Brazil, 2010, pp. 223–230.

[22] A. Kleiner, U. Kuhlmann, Experimental analysis of dual-steel bolted T-stubs under monotonic and cyclic loading, in: F. M. Mazzolani, G.-Q. Li, S. Chen, X. Qiang (Eds.), Proceedings of the Eighth International Conference on Behavior of Steel Structures in Seismic Areas (STESSA 2015), China Architecture & Building Press, Shanghai, China, 2015, pp. 1039–1046.

[23] M. S. Zhao, C. K. Lee, S. P. Chiew, Tensile behavior of high performance structural steel T-stub joints, Journal of Constructional Steel Research 122 (2016) 316–325.

[24] M. S. Zhao, S. P. Chiew, C. K. Lee, Post weld heat treatment for high strength steel welded connections, Journal of Constructional Steel Research 122 (2016) 167–177.

[25] M. S. Zhao, C. K. Lee, T. C. Fung, S. P. Chiew, Impact of welding on the strength of high performance steel T-stub joints, Journal of Constructional Steel Research 131 (2017) 110–121.

[26] C. Chen, X. Zhang, M. Zhao, C.-K. Lee, T.-C. Fung, S.-P. Chiew, Effects of welding on the tensile performance of high strength steel T-stub joints, Structures 9 (2017) 70–78.

[27] F. F. Sun, X. Y. Xue, Y. Xiao, Y. M. Le, G. Q. Li, Effect of welding and complex loads on the high-strength steel T-stub connection, Journal of Constructional Steel Research 150 (2018) 76–86.

[28] H. Guo, G. Liang, Y. Li, Y. Liu, Q690 high strength steel T-stub tensile behavior: Experimental research and theoretical analysis, Journal of Constructional Steel Research 139 (2017) 473–483.

[29] G. Liang, H. Guo, Y. Liu, Y. Li, Q690 high strength steel T-stub tensile behavior: Experimental and numerical analysis, Thin-Walled Structures 122 (2018) 554–571.

[30] G. Liang, H. Guo, Y. Liu, D. Yang, S. Li, A comparative study on tensile behavior of welded T-stub joints using Q345 normal steel and Q690 high strength steel under bolt preloading cases, Thin-Walled Structures 137 (2019) 271–283.

[31] T. Lin, Z. Wang, F. Hu, W. Hou, Comparison in tensile behaviour of conventional and high-strength steel welded-plate preloaded T-stubs, Structures 43 (2022) 93–104.

[32] Z. Chen, F. Gao, Z. Wang, Q. Lin, S. Huang, L. Ma, Performance of Q690 high-strength steel T-stub under monotonic and cyclic loading, Engineering Structures 277 (2023) 115405.

[33] Ministry of Housing and Urban-Rural Development of the People's Republic of China (MOHURD), Technical specification for high strength bolt connections of steel structures. JGJ 82-2011, China Building Industry Press, Beijing, China, 2011. (in Chinese).

[34] European Convention for Constructional Steelwork (ECCS), Recommended testing procedure for assessing the behavior of structural steel elements under cyclic loads. ECCS TWG 1.3 N. 45, European Convention for Constructional Steelwork, Brussels, Belgium, 2005.

[35] Applied Technology Council (ATC), Guidelines for cyclic seismic testing of components of steel structures. ATC-24, Applied Technology Council, Redwood City, California, USA, 1992.

[36] H. Krawinkler, M. Zohrei, Cumulative damage in steel structures subjected to earthquake ground motions, Computers & Structures 16 (1983) 531–541.

[37] C. Faella, V. Piluso, G. Rizzano, Cyclic behaviour of bolted joint component, Journal of Constructional Steel Research 46 (1998) Paper No. 129.

[38] C. Faella, V. Piluso, G. Rizzano, Structural steel semirigid connections: theory, design and software, CRC Press, Boca Raton, Florida, USA, 2000.

[39] V. Piluso, G. Rizzano, Experimental analysis and modelling of bolted T-stubs under cyclic loads, Journal of Constructional Steel Research 64 (2008) 655–669.

[40] V. Piluso, C. Faella, G. Rizzano, Ultimate behavior of bolted T-stubs. I: Theoretical model, ASCE Journal of Structural Engineering 127 (2001) 686–693.

[41] V. Piluso, C. Faella, G. Rizzano, Ultimate behavior of bolted T-stubs. II: Model validation, ASCE Journal of Structural Engineering 127 (2001) 694–704.